

# Electrical machines modeling for hybrid vehicle applications

Ing. N. HEINDRYCKX  
Ing. L. MINE  
Ing. D. ROUCHARD  
ECAM – Bruxelles

*Deux des moteurs électriques les plus prometteurs pour l'automobile hybride sont les moteurs asynchrones et les moteurs à réluctance variable. Pour leur conception, des modèles mathématiques précis sont nécessaires afin d'évaluer leurs performances avant de disposer du prototype. Diverses techniques de modélisation existent, dont le circuit magnétique équivalent. Nous appliquerons cette technique aux deux machines citées, évaluerons sa précision et tenterons de l'améliorer.*

*Mots-clefs : véhicule, voiture, hybride, machine, moteur, électrique, réluctance, variable, asynchrone, modélisation, circuit, magnétique, équivalent, éléments, finis.*

*Two of the most promising electric motors for hybrid vehicle applications are asynchronous motors and switched reluctance motors. For their design, accurate mathematical models are necessary to evaluate their performance before having the prototype. Various techniques of modelization exist, including the magnetic reluctance network. We will apply this technique to the two machines mentioned, evaluate its accuracy and try to improve it.*

*Keywords : vehicle, car, hybrid, machine, motor, electric, reluctance, variable, induction, modelization, circuit, magnetic, equivalent, elements, finite.*

## 1. Introduction

Electric machines (EMs) are indispensable components in different industrial drivetrains. Thanks to their robust control, induction machines (IMs) are still considered one of the most used EMs in industrial applications [1]. On the other side, switched reluctance motors (SRM's) and their unbeatable efficiency and power density could very soon disrupt the market [8].

In order to design EMs, accurate models are needed. Finite element (FE) is often used to model EMs. However, the computational time, as well as the huge memory usage, make the use of FE not preferable, especially in the early design phase where a lot of iterations are needed. On the other hand, lumped parameter models can be used, which are simple but lack the accuracy.

Alternatively, fast analytical models based on magnetic reluctance network (MRN) principle can be used. This technique was used to model two machines: IM and SRM. As FE results are infallible, they offer a good base to judge the quality of the MRN model. The models have been realized on the Matlab software.

The MRN principle is to convert a magnetic structure (i.e the rotor of an electric motor) in a network of interconnected flux tubes and reluctances. This magnetic circuit will then be solved in the same way as an electric circuit, applying Kirchoff laws.

MRN-modelling can be illustrated with the simple example of a coil making  $N$  turns around a rectangular frame (length “ $l$ ” and cross section “ $A$ ”) made of magnetic material (permeability  $\mu_r$ )

The following equations can be written [9]:

$$\mathcal{F} = NI$$

$$\mathfrak{R} = \frac{1}{\lambda} = \frac{l}{S\mu_0\mu_r}$$

$$\phi = \frac{\mathcal{F}}{\mathfrak{R}}$$

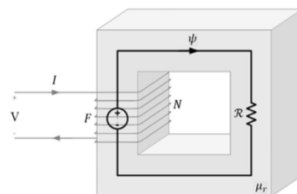


Figure 1: Magnetic circuit

## 2. SRM

### 2.1. Introduction

SRM's, standing it a passive rotor an active stator, have an easy working principle: When 2 opposite stator pole windings are powered, magnetic induction  $B$  appears, a flux is created.

When a magnetically salient rotor is subject to the flow of flux in the magnetic circuit, it tends to rotate toward the position of minimum reluctance. Because of the relation  $\mathcal{F} = \mathcal{R}\phi$  moving to the minimum reluctance position means also to move in order to maximize the flux  $\phi$  thus moving to the powered pole. When finally 2 rotor poles are aligned with the powered stator poles, the reluctance is minimum and the rotor will stay at this place, producing 0 torque. It is therefore time to power 2 other opposite stator pole windings, which not have rotor pole aligned with them, to continue the rotation of the rotor. [11]

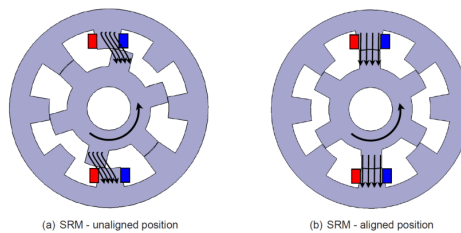


Figure 2: SRM principle

The fact that each stator pole produces consecutively an independent torque, combined with the highly symmetry of the machines, makes the SRM particularly suitable for MRN-based models. We can effectively model the values for one pole, and then extrapolate them for the other poles and thus for the whole rotation.

However, getting a precise MRN model of an SRM is still a challenge, namely for what concerns the air gap reluctance values and the non-linear permeability of the magnetic material which requires an iteration process. We will here discuss about the precision of the obtained model through a FE comparison, as well as the applied (or no) ways of improvement.

First, the solving of the MRN network of the SRM's will be tackled. Secondly, its precision will be discussed through a FE comparison. Finally, conclusions are made, and we will discuss the possible future improvements.

## 2.2. MRN model

The model should be parametrized and thus work with any number of stator and rotor poles. By designing only one pole phase of the motor and shifting the characteristic curves for other pole phases in function of their number, this MRN is universal.

The SRM's MRN consists in 4 main ferromagnetic parts: The stator yoke, the rotor yoke, the stator pole, the rotor pole.

When adding the 2 air gaps between the rotor and stator poles, we obtain the circuit represented on the figures bellows. Further simplification can be done by summing similar reluctances [10]:

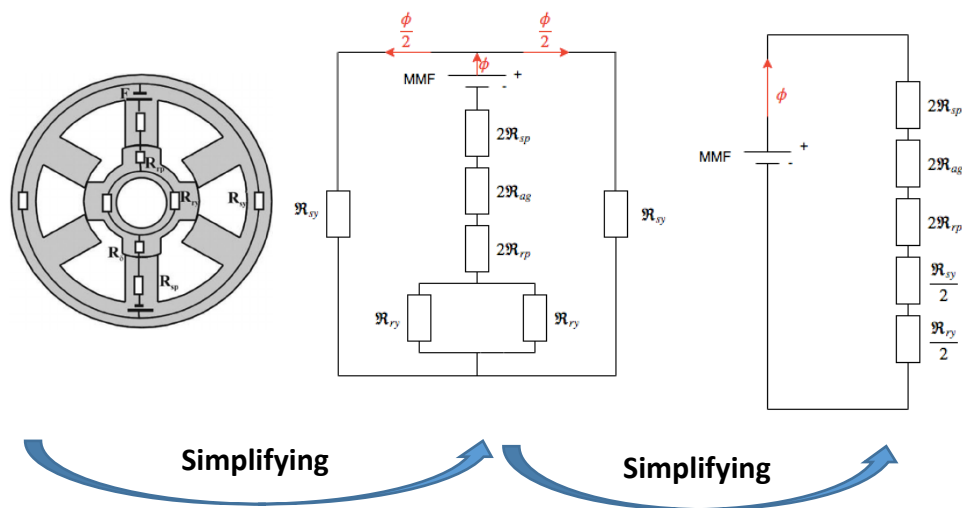
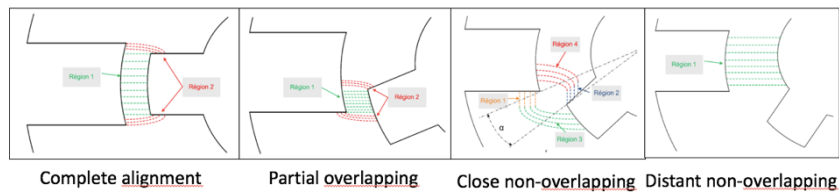


Figure 3: MRN simplification

The first reluctance to be calculated is the air gap reluctance and its calculation is complicated since position dependent. First, different phases are assumed to be independent. Next, the model is divided into 4 regions according to the position of the rotor regarding the position of the stator [10]:



An air gap permeance is for each region calculated by  $\lambda = \mu_0 S l^{-1}$  with  $S$ , cross section of the flux lines and  $l$ , length of the flux lines. Both of these variables are in the model dynamic functions of  $\theta$ , the rotor position angle. By gathering those different reluctances, we can assemble the matrix of the total air gap permeance. The figure below represent the evolution of the air gap permeance evolution around one pole. This evolution applies on every stator pole of the SRM since it is highly symmetric.

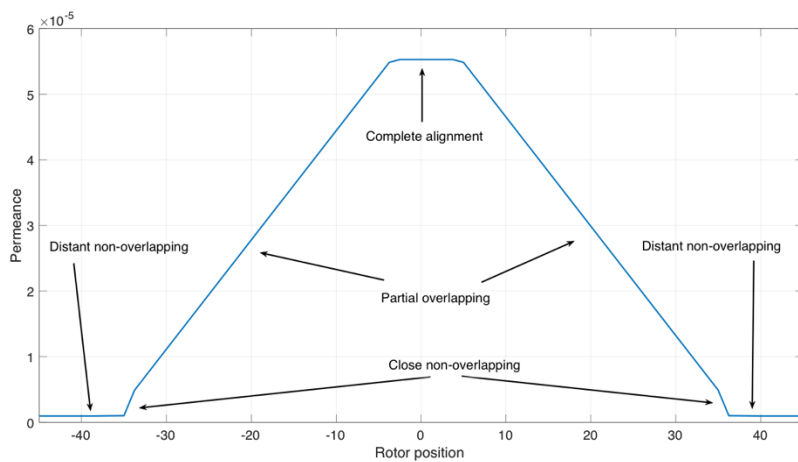


Figure 4: Air gap reluctance

The next reluctances to compute from our MRN are the stator yoke reluctance, the rotor yoke reluctance, the stator pole reluctance and the rotor pole reluctance. The formula is again given by  $\lambda = \mu S l^{-1}$  but this time  $S$  and  $l$  are constant values. On the other hand, because of the saturation of the magnetic parts of the motor, the magnetic permeability  $\mu$  is not constant and the following loop has to be taken in account:

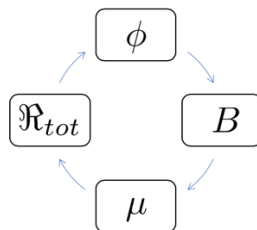


Figure 5: Iterative loop

The following iterative schema has therefore been implemented in the model. "Tol" is the tolerance value for the iterations: when the step value is lower than "tol", iterations will stop and the last result of the  $\phi$  matrix will be considered correct.

The flux  $\phi$  is given by  $\phi = 2 * NrWindings * \mathcal{F} \mathfrak{R}^{-1}$  with the magnetomotive force  $\mathcal{F} = 2 * nWindings * Current$ . A factor 2 is applied because 2 poles are active. [9]:

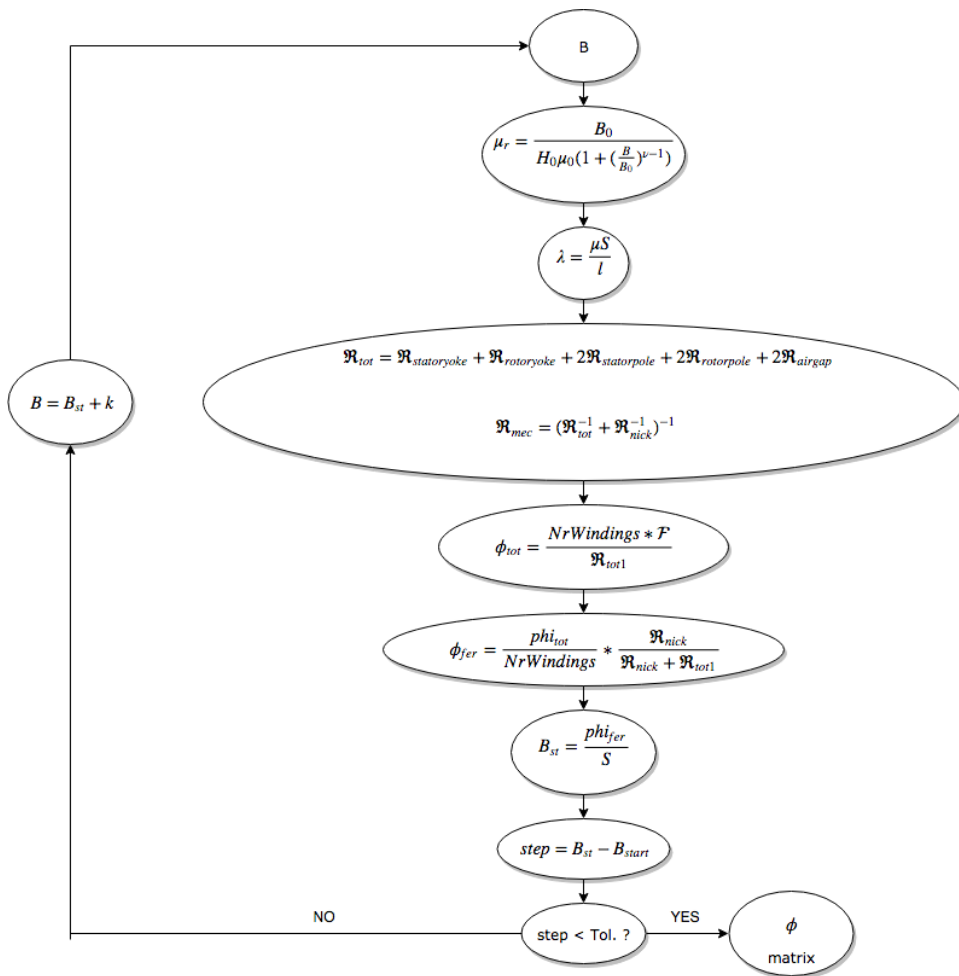


Figure 6: Iterative scheme

With “ $i$ ”, the applied current and “ $\theta$ ” the rotor position, the obtained  $\varphi$  matrix leads through the following formula to the torque matrix:

$$T = \frac{\partial W'}{\partial \theta} = \frac{(\sum_{j=0}^{i_2} \phi_j * i_2) - (\sum_{j=0}^{i_1} \phi_j * i_1)}{\theta_2 - \theta_1}$$

### 2.3. Results precision analysis

The precision of the model can be highlighted by testing it with different topologies and dimensions of machines and comparing the obtained MRN results with FE results. In particular, the “8/6” and “6/4” topologies were tested. This means that in the first case, the machine stands in 8 stator poles and 6 rotor poles, and in the second case, 6 stator poles and 4 rotor poles.

A first sample of the relative permeability result shows a slight difference with the finite elements results. The iterative scheme higher the value faster than it should.

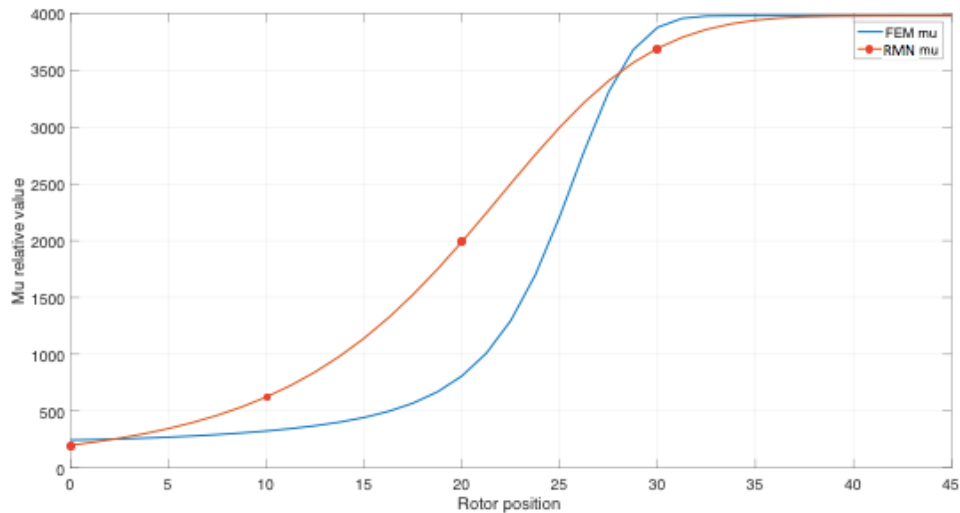


Figure 7: Mu values comparison

It will result on overestimated flux values. But as the torque only depends on the flux variations, we can still expect a good accuracy on the overall machine behaviour, which is confirmed by the torque curves analysis:

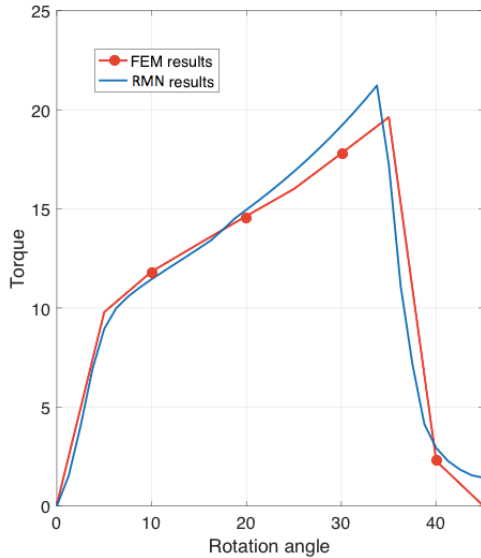


Figure 9: 6/4 SRM - Linear conditions

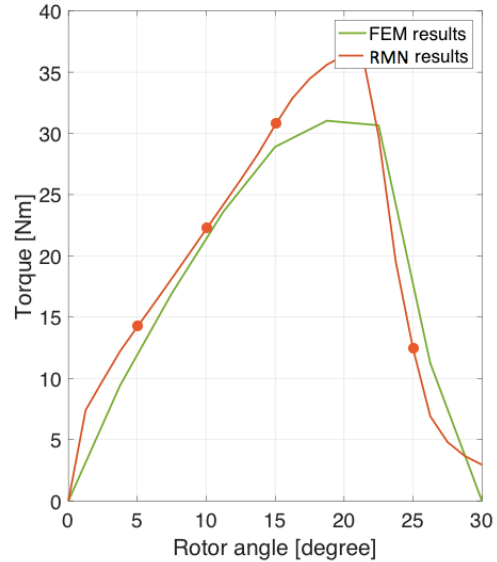


Figure 8: 8/6 SRM - non-linear conditions

## 2.4. Conclusions

The realized MRN model gives a good approximation of the overall performances of the SRM in less than 0.2s, which is easily 150 times faster than a FE model. The correctness of the output torque values have been repeatable over 2 motors of different topologies.

On the other hand, there is still room for improvement in the permeability values. The iterative scheme for the relative permeability in the magnetic parts can be improved, but the main problem remains the air gap reluctance which is reputed as being very difficult to modelize for the SRM's. A way to increase the precision of the model would then be to use a FE model only for this reluctance, and the RMN for all the other magnetic values of the machine.

It could lead to a good compromise between computation time and precision.

### 3. Induction Machine

#### 3.1. Introduction

The MRN models of IMs were previously presented in literature, see for example [2]. However, the implementation of these models is not straight-forward for IM's. For example, a lot of tuning is needed to overcome the matrices bad conditioning. In this work, an efficient approach was provided to improve the quality of the MRN dynamic models of IMs. In order to validate the developed approach, a comparison with FE results is given.

In the subsequent section, an overview about the MRN of IMs is given. In the third section, the proposed model improvement is shown and explained. The use case and the associated analysis, including validation using the FE model, is discussed in section 4. Finally, the conclusions are drawn in section 5.

#### 3.2. MRN model

Basically, the MRN of any electromagnetic device is constructed in such a way that each geometrical part of the magnetic circuit, in which a uniform field pattern may be assumed, is replaced by its corresponding reluctance element, while the electromagnetic sources can be represented by lumped magnetomotive forces (MMF), see Fig. 1 where a schematic diagram of the MRN of an IM is shown.

The methodology detailed in this paragraph has already been presented in [2]. Therefore, the novelty of this present work is not related to the MRN approach itself, but rather to the improvement of such dynamic model so as to reduce the model complexity.

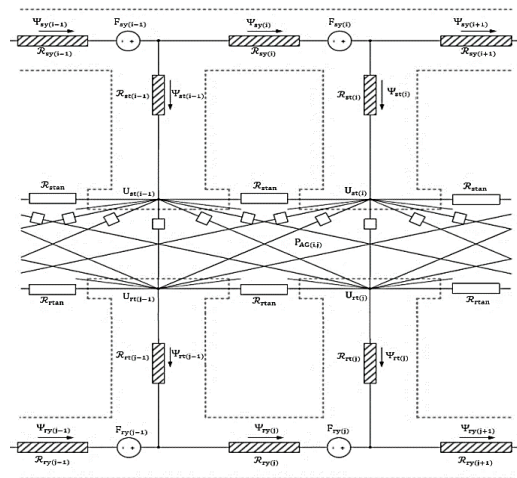


Figure 10 : Schematic diagram of the MRN of a squirrel-cage IM.

By the analogy between electric and magnetic circuits [3], the equivalent MRN circuit can be analyzed using Kirchhoff's current (KCL) and voltage laws (KVL) which leads to equation (1) modeling the magnetic behaviour of the machine:

$$A_{magn} X_{magn} = Y_{magn} \quad (1)$$

$$\begin{bmatrix} \mathbf{M1} & \mathbf{0} & A_{ust} & \mathbf{0} \\ \mathbf{0} & \mathbf{M2} & \mathbf{0} & A_{urt} \\ -A_{syt} & \mathbf{0} & A_{ss} & A_{sr} \\ \mathbf{0} & -A_{ryt} & A_{rs} & A_{rr} \end{bmatrix} \begin{bmatrix} \Psi_{sy} \\ \Psi_{ry} \\ U_{st} \\ U_{rt} \end{bmatrix} = \begin{bmatrix} F_{sy} \\ F_{ry} \\ \mathbf{0} \\ \mathbf{0} \end{bmatrix}$$

where  $X_{magn}$ ,  $A_{magn}$ , and  $Y_{magn}$  are respectively the vector of magnetic unknowns (containing the stator and rotor yoke fluxes ( $\Psi_{sy}, \Psi_{ry}$ ) and the stator and rotor node potentials ( $U_{st}, U_{rt}$ )), the matrix of magnetic coefficients (where  $\mathbf{M1}$  and  $\mathbf{M2}$  are matrices containing the MRN core reluctances,  $A_{ss}$ ,  $A_{sr}$ ,  $A_{rs}$  and  $A_{rr}$  are matrices containing the MRN airgap permeances and  $A_{syt}$ ,  $A_{ryt}$ ,  $A_{ust}$ ,  $A_{urt}$  are coefficient matrix composed by ones and zeros) and the input vector containing the stator and rotor yoke MMFs  $F_{sy}$  and  $F_{ry}$ .

By using Faraday's, Lenz's and Ampere's laws, this magnetic model can be linked to the electrical circuits of the machine. Ampere's law allows to find a relation between the MMFs in the yokes and the current in the corresponding slot (i.e. stator currents and rotor bar currents). In addition, Faraday's and Lenz's laws were used to take the voltage drop created by flux linkage variation into account on the stator coils and to generate equations for the rotor electric meshes.

A linear model of the IM can then be described using matrix-equation (2), where  $X$ ,  $A$ , and  $Y$  are respectively the vector of unknowns (containing the vector of magnetic unknowns ( $X_{magn}$ ), stator currents ( $I_s$ ) and rotor ring currents ( $I_r$ )), the matrix of coefficients and the vector of input, i.e. stator voltage waveform. In the matrix of coefficients, one can find the MMF and the flux connection matrices ( $W_{cs}$  and  $M_{efs}$ , which both depend on the winding distribution and the number of turns of the stator coils) and the stator and rotor resistance matrices ( $R_s$  and  $\mathbf{M3}$ , respectively). For more details, see [2].

$$\begin{array}{c}
AX = Y \\
\left[ \begin{array}{cccccc}
M_{cfs} A_{syt} & \mathbf{0} & \mathbf{0} & \mathbf{0} & \frac{dt}{2} R_s & \mathbf{0} \\
\mathbf{0} & -A_{ryt} & \mathbf{0} & \mathbf{0} & \mathbf{0} & M3 \frac{dt}{2} \\
M1 & \mathbf{0} & A_{ust} & \mathbf{0} & -W_{cs} & \mathbf{0} \\
\mathbf{0} & M2 & \mathbf{0} & A_{urt} & \mathbf{0} & A_{ryt} \\
-A_{syt} & \mathbf{0} & A_{ss} & A_{sr} & \mathbf{0} & \mathbf{0} \\
\mathbf{0} & -A_{ryt} & A_{rs} & A_{rr} & \mathbf{0} & \mathbf{0}
\end{array} \right] \begin{bmatrix} \Psi_{sy} \\ \Psi_{ry} \\ U_{st} \\ U_{rt} \\ I_s \\ I_r \end{bmatrix} = \begin{bmatrix} Y1 \\ Y2 \\ \mathbf{0} \\ \mathbf{0} \\ \mathbf{0} \\ \mathbf{0} \end{bmatrix}
\end{array} \quad (2)$$

with:

$$\begin{aligned}
Y1 &= (V_s + V_{s(t-1)} - R_s I_{s(t-1)}) \frac{dt}{2} + M_{cfs} A_{syt} \Psi_{sy(t-1)} \\
Y2 &= -A_{ryt} \Psi_{ry(t-1)} - M3 \frac{dt}{2} I_{r(t-1)}
\end{aligned}$$

The obtained electromagnetic model can then be linked to the mechanics of the machine using (3) based on electromechanical energy conversion principle [3], where  $\tau_e$  is the electromagnetical torque,  $P_{AG(i,j)}$ , the airgap permeance between the  $i$ -th stator tooth and the  $j$ -th rotor tooth, and the rotor angular position  $\theta_m$ .

$$\tau_e = 0.5 \sum_{i=1}^{N_s} \sum_{j=1}^{N_r} (U_{s(i)} - U_{r(j)})^2 \frac{dP_{AG(i,j)}}{d\theta_m} \quad (3)$$

Finally, in order to consider the core saturation in the model, the permeability of the iron in each reluctance of the MRN needs to be related to the flux density passing through it. In this work, an equation based on two parameters (i.e.  $a$  and  $b$ ) is used for saturation effect modeling and is presented in (4) [2]:

$$H(B) = \frac{\sqrt{\pi} \operatorname{Erfi}(|B|\sqrt{-a})}{2b\sqrt{-a}} \quad (4)$$

When core saturation is considered, there is a circular relation between flux density, permeability and core reluctances of the MRN. An iterative method is needed and Newton-Raphson (NR) successive approach is well suited for that purpose [4]. Therefore, the non-linear model of the IM becomes:

$$\begin{cases} d\mathbf{X}_{k-1} = (\mathbf{J}_{k-1})^{-1} (\mathbf{A}_{k-1} \mathbf{X}_{k-1} - \mathbf{Y}_{k-1}) \\ \mathbf{X}_k = \mathbf{X}_{k-1} + d\mathbf{X}_{k-1} \end{cases} \quad (5)$$

where  $k$  is the iteration identifier and  $\mathbf{J}_{k-1}$  is the Jacobian matrix. In the following section, the two techniques improving the model's accuracy will be shown.

### 3.3. Conditioning improvement

Due to bad conditioning, the inversion of the Jacobian matrix  $J_{k-1}$  is often imprecise and may produce numerical troubles. This bad conditioning is especially a problem when the motor operates in highly saturated conditions, the Jacobian matrix then becomes singular for inversion and the NR algorithm may not converge. Therefore, we propose a reduction technique to avoid this bad conditioning problem and improve the model accuracy.

We have observed that  $I_s$  and  $I_r$  are dependent states that can be extracted from the  $X$  vector. The linear model of the IM then becomes (6):

$$\begin{bmatrix} -A_{syt} & \mathbf{0} & A_{ss} & A_{sr} \\ \mathbf{0} & -A_{ryt} & A_{rs} & A_{rr} \\ A_1 & \mathbf{0} & -A_{ust} & \mathbf{0} \\ \mathbf{0} & A_2 & \mathbf{0} & -A_{urt} \end{bmatrix} \begin{bmatrix} \Psi_{sy} \\ \Psi_{ry} \\ U_{st} \\ U_{rt} \end{bmatrix} = \begin{bmatrix} \mathbf{0} \\ \mathbf{0} \\ \frac{2 \cdot R_s^{-1} W_{cs} Y1}{dt} \\ -\frac{2 \cdot A_{ryt} M3^{-1} Y2}{dt} \end{bmatrix} \quad (6)$$

with:

$$A_1 = \frac{2}{dt} R_s^{-1} W_{cs} M_{cfs} A_{syt} + M1$$

$$A_2 = \frac{2}{dt} A_{ryt} M3^{-1} A_{ryt} + M2$$

The two extracted state vectors can be calculated afterwards by means of the remaining states, obtained by NR algorithm, by using (7) and (8).

$$I_s = \frac{2}{dt} R_s^{-1} (M_{cfs} A_{syt} \Psi_{sy} + Y1) \quad (7)$$

$$I_r = \frac{2}{dt} M3^{-1} (A_{ryt} \Psi_{ry} + Y2) \quad (8)$$

Reducing vector  $X$  will also reduce coefficient matrix  $A$ , i.e. less spars and smaller matrix which leads to a better convergence and a faster computation. With a reduced model, the Jacobian matrix  $J_{k-1}$  can be presented as (9):

$$J_{k-1} = \begin{bmatrix} -A_{syt} & \mathbf{0} & A_{ss} & A_{sr} \\ \mathbf{0} & -A_{ryt} & A_{rs} & A_{rr} \\ A_1 + \frac{d(M1\Psi_{sy})}{d\Psi_{sy}} & \mathbf{0} & -A_{ust} & \mathbf{0} \\ \mathbf{0} & A_2 + \frac{d(M2\Psi_{ry})}{d\Psi_{ry}} & \mathbf{0} & -A_{urt} \end{bmatrix} \quad (9)$$

The derivative of matrix  $\mathbf{M1}\Psi_{sy}$ , with respect to the stator yoke fluxes ( $\Psi_{sy}$ ) is shown in (10). To obtain the derivative of the  $\mathbf{M2}\Psi_{ry}$  matrix over the rotor yoke fluxes  $\Psi_{ry}$ , the elements of stator (10) need to be replaced by their correspondent rotor elements, i.e.  $dA_{\Psi_{st}}/d\Psi_{sy}$ ,  $dA_{\Psi_{sy}}/d\Psi_{sy}$ ,  $\Psi_{sy,d}$  and  $\mathbf{M1}$  have to be replaced by  $dA_{\Psi_{rt}}/d\Psi_{ry}$ ,  $dA_{\Psi_{ry}}/d\Psi_{ry}$ ,  $\Psi_{ry,d}$  and  $\mathbf{M2}$  respectively.

$$\frac{d(\mathbf{M1}\Psi_{sy})}{d\Psi_{sy}} = \left( \frac{dA_{\Psi_{st}}}{d\Psi_{sy}} + \frac{dA_{\Psi_{sy}}}{d\Psi_{sy}} \right) \Psi_{sy,d}$$

with:

$$\frac{dA_{\Psi_{st}}}{d\Psi_{sy}} = \begin{bmatrix} \frac{d\mathcal{R}_{st(1)}}{d\Psi_{sy(1)}} - \frac{d\mathcal{R}_{st(N_s)}}{d\Psi_{sy(N_s)}} & \frac{d\mathcal{R}_{st(1)}}{d\Psi_{sy(1)}} & \dots & -\frac{d\mathcal{R}_{st(N_s)}}{d\Psi_{sy(N_s)}} \\ -\frac{d\mathcal{R}_{st(1)}}{d\Psi_{sy(1)}} & \frac{d\mathcal{R}_{st(2)}}{d\Psi_{sy(2)}} - \frac{d\mathcal{R}_{st(1)}}{d\Psi_{sy(1)}} & \dots & 0 \\ \vdots & \vdots & \ddots & \vdots \\ 0 & 0 & \dots & \frac{d\mathcal{R}_{st(N_s-1)}}{d\Psi_{sy(N_s-1)}} \\ \frac{d\mathcal{R}_{st(N_s)}}{d\Psi_{sy(N_s)}} & 0 & \dots & \frac{d\mathcal{R}_{st(N_s)}}{d\Psi_{sy(N_s)}} - \frac{d\mathcal{R}_{st(N_s-1)}}{d\Psi_{sy(N_s-1)}} \end{bmatrix} \quad (10)$$

$$\frac{dA_{\Psi_{sy}}}{d\Psi_{sy}} = \begin{bmatrix} \frac{d\mathcal{R}_{sy(1)}}{d\Psi_{sy(1)}} & \dots & 0 \\ \vdots & \ddots & \vdots \\ 0 & \dots & \frac{d\mathcal{R}_{sy(N_s)}}{d\Psi_{sy(N_s)}} \end{bmatrix} \quad \text{and} \quad \Psi_{sy,d} = \begin{bmatrix} \Psi_{sy(1)} & \dots & 0 \\ \vdots & \ddots & \vdots \\ 0 & \dots & \Psi_{sy(N_s)} \end{bmatrix}$$

In addition to this reduction technique, the inversion of the Jacobian matrix presented in (9) can be damped. In other words, a Levenberg-Marquardt coefficient ( $c$ ) can be added to the diagonal of the  $\mathbf{J}_{k-1}$  matrix to smooth the inversion process [5]. The value of  $c$  coefficient needs to be carefully chosen as a trade-off between stability and precision.

### 3.4. Simulation results and validation

In this section, simulation and validation are shown with a 2 pair of poles 36/28 slots IM of 1500 W with parameters presented in table I. Corresponding dimensions are shown on the schematic cross-section, see Fig. 2. The magnetic core is modelled using the saturation curve shown in Fig. 3 obtained by using the two next constants:

$$a = -0.8, b = 1000 \quad (11)$$

TABLE I Machine properties

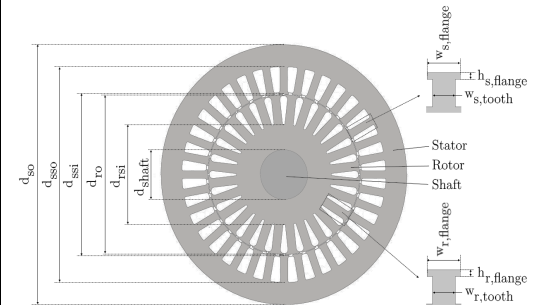
2P-36/28 IM – 1500 W			
<b>Dimen- sions</b>	$d_{so} = 130$ mm	$d_{ro} = 80$ mm	
	$d_{sso} = 108$ mm	$d_{rsi} = 50$ mm	
	$d_{ssi} = 80.76$ mm	$d_{shaft} = 25$ mm	
	$h_{sfl} = 0.64$ mm	$h_{rfl} = 0.5$ mm	
	$w_{sfl} = 5.05$ mm	$w_{rfl} = 7.98$ mm	
	$w_{st} = 3.8$ mm	$w_{rt} = 4.4$ mm	
$l_{motor} = 100$ mm			
<b>Electric parame- ters</b>	$N_s = 36$	$N_r = 28$	
	$R_{stat} = 5$ $\Omega$	$R_{ring} = 8.1$ m $\Omega$	
	$N = 44$ turns/slot	$R_{bar} = 74$ m $\Omega$	

Fig. 12: Schematic diagram of the machine geometry

Fig. 4 to Fig. 7 depict the dynamic behaviour of the machine in saturated conditions. The motor is fed by a 200 V, 50 Hz voltage and the load-torque ( $\tau_L$ ) is considered as squarely dependent on the rotor speed ( $\omega_m$ ):

$$\tau_L = 35 \cdot 10^{-5} \cdot \omega_m^2 \quad (12)$$

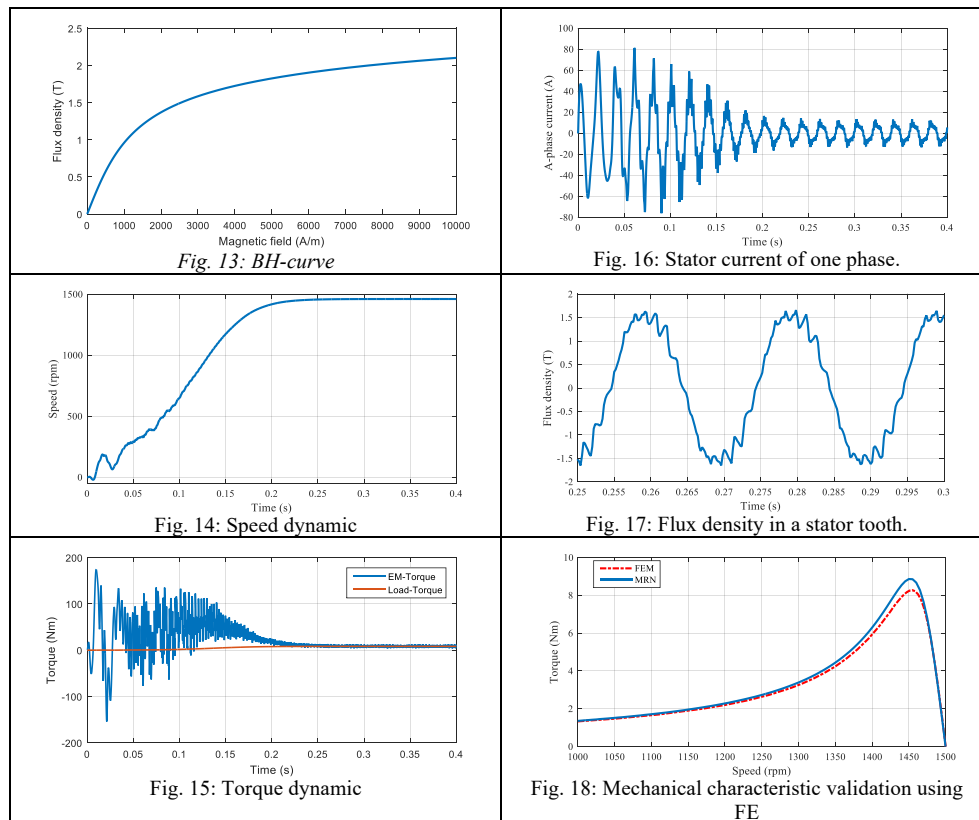
The transient speed behaviour of the simulation results can be observed in Fig. 4, while the electromagnetic and load torques are presented in Fig. 5. The steady-state operating point of this simulation is at 1461 rpm and 8.19 Nm. The stator current of phase A in time domain is depicted in Fig. 6, it reaches a peak value 13.65 A in steady-state. In addition, in Fig. 7 the stator tooth flux density is presented in steady-state. It can be observed that the maximum reached flux density is around 1.68 T, which is at the knee point defined by the  $B$ - $H$  curve, see Fig. 3. This shows the non-linearity is properly considered.

The presented MRN model was validated using FEM and showed a good accuracy as can be observed on the torque versus speed characteristic (Fig. 8). On the other hand, the computation time is strongly reduced when using MRN method rather than FEM. The showed validation was obtained by keeping a 5 A peak in the stator coils while making the speed vary between 1000 and 1500 rpm.

Due to its accuracy and low computation time, the MRN model can be used for online fault detection. The current spectrum can be analysed to detect broken bars in the squirrel cage [6] or inter-turn short circuits in the stator coils [2].

The model can also be used for efficiency map generation. Since a lot of operating points are needed to draw the efficiency map, a low computation time is required to obtain quick results. Efficiency can be obtained from the MRN model by the use of loss computation. Joule losses can be calculated from the currents and the iron loss from the flux densities by the use of separation principle [7]. To speed up the results, as well as to ease the implementation of the field-oriented control, this load-voltage

input model can be transformed into a speed-current input model by switching current and voltage from input to unknown and by putting the speed directly as input of the model. This makes it possible to lower the transient time of simulation and reach faster steady-state from which efficiency can be computed.



### 3.5. Conclusions

Two simple techniques were presented in this part in order to improve the transient MRN-model of a squirrel cage induction machine. The two techniques are based on reducing the system complexity by re-arranging the matrices, and speed up the convergence process by choosing a proper damping coefficient. The improved model is applied into a three-phase IM, with acceptable results validated by FE technique (5.2% error). It is worth mentioning that the developed model can be used in different applications, such as fault detection. Also, it is quite easy to invert the model input from voltage source to current source that may result in quick steady-state results.

Finally, we would like to thank the FlandersMake company for welcoming us during 10 months in the context of this research.

## 4. References

- [1] A. Zabardast and H. Mokhtari, “Effect of high-efficient electric motors on efficiency improvement and electric energy saving,” DRPT, China, 6-9 April 2008.
- [2] P. Naderi, “Inter-turn short-circuit fault detection in saturable squirrel-cage induction motor using magnetic equivalent circuit model,” *COMPEL*, vol. 35, issue 1, pp. 245-269, 2016.
- [3] V. Ostovic, *Dynamics of saturated electric machines*. Springer, 1989.
- [4] G. Crevecoeur, *Numerical Methods for Low Frequency Electromagnetic Optimization and Inverse Problems Using Multi-Level Techniques*. PhD Thesis, Ghent University, Belgium, May 2009.
- [5] J. E. Gentle, *Matrix Algebra: Theory, Computations and Applications in Statistics*. Springer, 2017.
- [6] N. A. O. Demerdash, A. Sayed-Ahmed, G. Y. Sizov, C. Yeh, “Analysis and Diagnostics of Adjacent and Nonadjacent Broken Rotor Bar Faults in Squirrel-Cage Induction Machines,” *IEEE Transactions on Industrial Electronics*, vol. 56, no. 1, pp. 4627-4641, 2009.
- [7] G. Bertotti, “General properties of power losses in soft ferromagnetic materials,” *IEEE Transactions on Magnetics*, vol. 24, no. 1, pp. 621–630, 1988.
- [8] “Switched reluctance motor aims to disrupt the market”, 27 February 2018, unknown, consulted on <http://drivesncontrols.com/news> the 30 September 2018.
- [9] A. M. A. Abdallah, “An Inverse Problem Based Methodology with Uncertainty Analysis for the Identification of Magnetic Material Characteristics of Electromagnetic Devices”, PhD, Ghent University, 2012
- [10] Dan Ilea, « Conception optimale des moteurs à réluctance variable à commutation électronique pour la traction des véhicules électriques légers », PhD, Université de Lille, 2011
- [11] Lluís Colomo Guilera, “Analytical design of a Synchronous Reluctance motor (SRM)”, thesis, Treball de Fi de Grau, 2018